Microwave imaging based on two hybrid particle swarm optimization approaches

Bouzid Mhamdi

Syscom Laboratory, Engineer School of Tunis, BP 37 Belvedere, Tunis - 1002, Tunisia

Abstract

In this paper, the solution of the inverse scattering problem for determining the shape and location of perfectly conducting scatterers by making use of electromagnetic scattered fields is presented. Based on the boundary condition and the measured scattered field, a set of nonlinear integral equations is derived and the imaging problem is reformulated into an optimization one. Then, two evolutionary algorithms are used to solve the inverse scattering problem. To further clarify, our contribution is to test two well-known algorithms in the literature to the problem of microwave imaging. The hybrid approaches combine the standard particle swarm optimization (PSO) with the ideas of the simulated annealing and extremal optimization algorithms, respectively. Both of them are shown to be more efficient than original PSO technique. Reconstruction results by using the two presented schemes are compared with exact shapes of some conducting cylinders; and good agreements with the original shapes are observed.

Introduction

The aim of electromagnetic inverse scattering problem is to recover the shape and/or electromagnetic properties concerning some inaccessible regions from the scattered electromagnetic fields measured outside. Over the last few years, microwave imaging techniques have attracted considerable attention from the research community since they can be suitably used for a number of engineering applications ranging from medical diagnostics to nondestructive evaluation and subsurface detection. However, inverse problems of this type are difficult to solve because of its ill-posedness and nonlinearity [1]. A large number of methods have been proposed to solve the inverse scattering problem and the inversion is formulated as an optimization problem.

Traditional iterative algorithms are founded on local minimization of an objective function via some gradient-scheme [2, 3]. Generally, during the search of the global minimum, they only converge under certain conditions, otherwise, they may be trapped into a local extreme or even diverge. More recently, a new class of algorithms has emerged such as simulated annealing (SA) [4], neural network [5], genetic algorithms (GA) [6–8], and differential evolution [9–13]. In recent year, some researchers have focused on applying the particle swarm optimization (PSO) [14] in solving inverse scattering problem [15–20].

Researchers are still relying on the previously mentioned methods to find appropriate solutions to the microwave imaging problem.

But all this does not mean to mention the basic drawbacks of all these used methods, namely, the premature convergence for the global stochastic optimization techniques and the convergence to the local minimum solution for the local optimization methods.

Based on what has been said, we have thought in this work to overcome all these drawbacks using a hybrid method which combines the two types together. PSO can be easily implemented and is computationally inexpensive in terms of both memory requirements and CPU speed [21]. However, even though PSO is a good and fast search algorithm, it has premature convergence.

To avoid premature convergence of PSO, an idea of combining PSO with SA is addressed in this paper; the rationale behind is that such a hybrid approach expects to enjoy the merits of PSO with those of SA. In other words, PSO contributes to the hybrid approach in a way to ensure that the search converges faster, while the SA makes the search to jump out of local optima.

In order to solve the complex inverse scattering problem, we employ in this work a hybrid optimization method called PSOSA which is already reported in the literature [22]. To the best of our knowledge, there is still no investigation on using hybrid technique based on PSO and SA to reconstruct an arbitrary shape of conducting cylinders in free space. In addition to PSOSA, we apply another hybrid technique called PSOEO combining PSO with a local search heuristic algorithm named extremal optimization (EO). This PSOEO algorithm is quite detailed in [23].

The remaining sections of this paper are organized as follows: "Theoretical formulation" presents the formulation of the problem. A description of the hybrid algorithms structure is

given in "Hybrid algorithms, PSOSA, and PSOEO". The numerical results are discussed in "Numerical results" and finally "Conclusion" summarizes the study.

Theoretical formulation

Consider a perfect electrically conducting cylinder embedded in a free space as shown in Fig. 1. The cylinder is assumed infinite long in the z direction, while the cross-section of the cylinder is arbitrary. The scatterer is illuminated by a circumference source of pulsed plane waves, with z-polarized incident electric field E_z^i (TM polarization) and a propagation direction in the (x, y) plane and impinges at an incident angle φ_i. The z polarized incident wave can be given by:

$$E_z^i(x, y) = e^{-jK_0(x \cdot \cos \varphi_i + y \cdot \sin \varphi_i)}, \tag{1}$$

where K_0 denotes the free-space wave number.

Forward problem

In this work, the shape function of the object is assumed to be described by means of a Fourier series of order P:

$$\rho(\varphi) = \sum_{n=0}^{P} a_n \cos(n\varphi) + \sum_{n=1}^{P} b_n \sin(n\varphi). \tag{2}$$

a_n and b_n represent the Fourier coefficients:

$$a_n = \frac{1}{\pi} \int_0^{2\pi} \rho(\varphi) \cos(n\varphi) d\varphi, \tag{3}$$

$$b_n = \frac{1}{\pi} \int_0^{2\pi} \rho(\varphi) \sin(n\varphi) d\varphi. \tag{4}$$

Due to the homogeneity of the scatterer along the z-axis, the problem is reduced to a TM scalar case. The scattered and total electric fields will be polarized parallel to the z-axis. Surface current J_z is induced on the surface of the cylinder; the scattered electric field E_z^s is subsequently generated.

Starting from Maxwell's equations, an integral equation of first kind may be derived in which the scattered field E_z^s is given as:

$$E_z^s(\vec{r}) = -\frac{K_0 \eta}{4} \int_C J_z(\vec{r}') H_0^1(K_0 |\vec{r} - \vec{r}'|) ds(\vec{r}'), \tag{5}$$

where J_z is the induced current density parallel to the z-axis, η is the impedance of the surrounding medium, and H_0^1 is the Hankel function of the first kind and zeroth order.

At the surface of the cylinder, the total electric field satisfies the boundary condition:

$$E_z^i + E_z^s = 0. \tag{6}$$

Considering that $\vec{r} = (\rho(\varphi), \varphi)$ on contour C, if we combine (5) and (6), one obtains:

$$E_z^i(\rho(\varphi), \varphi) = \frac{K_0 \eta}{4} \int_0^{2\pi} J_z(\varphi') H_0^1(K_0 \delta) \xi d\varphi', \tag{7}$$
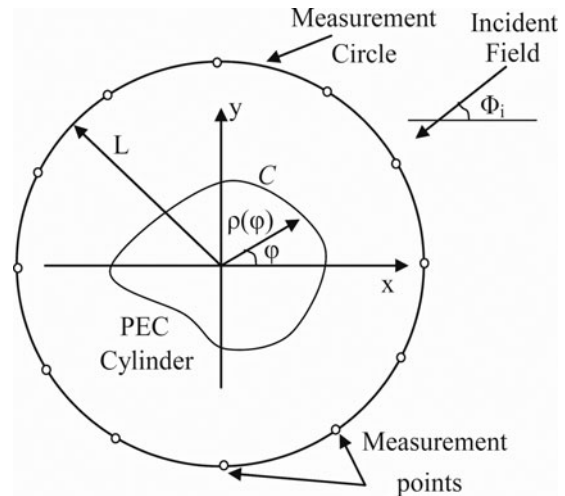

Fig. 1. Geometry of the considered inverse scattering problem in the (x, y) plane.

where

$$\delta = \sqrt{\rho^2(\varphi) + \rho^2(\varphi') - 2\rho(\varphi)\rho(\varphi') \cos(\varphi - \varphi')}, \tag{8}$$

$$\xi = \sqrt{\rho^2(\varphi') + \rho'^2(\varphi')}. \tag{9}$$

The distribution of surface current is obtained after solving equation (7) by point-matching method [24] with pulse basis function and Dirac delta test function. The contour C of the cylinder is divided into Q segments and the current density is assumed to be constant in each segment. A matrix equation is obtained:

$$AJ_z = B. \tag{10}$$

The elements of A and B are given in [25]. The elements of J_z represent the discrete electric currents on the sections of the counter C. Thus, the scattered field is calculated by using the discrete electric currents as follows:

$$E_z^s(r, \varphi) = -\frac{\omega\mu_0}{4} \Delta\varphi \sum_{n=1}^{Q} J_n H_0^{(1)}(K_0 \delta_n) \xi_n, \tag{11}$$

where $\Delta\varphi$ is the angular discretization size, δ_n and ξ_n are given as follows:

$$\delta_n = \sqrt{r^2 + \rho^2(\varphi_n) - 2r\rho(\varphi_n) \cos(\varphi - \varphi_n)}, \tag{12}$$

$$\xi_n = \sqrt{\rho^2(\varphi_n) + \rho'^2(\varphi_n)}. \tag{13}$$

According to (11), the scattered field depends on the Fourier coefficients which describe the object shape.

Inverse scattering problem

For the inverse problem, the scattered electric field is measured and known at each receiver while the shape function, i.e. the coefficients of the trigonometric series to be determined a_n and b_n are unknown. A relative error function J with respect to the

coefficients of the trigonometric series is defined as follows:

$$J(X) = \frac{\sqrt{\sum_{n=1}^{M \times S} |(E^s_{meas})_n - (E^s_z)_n|^2}}{\sqrt{\sum_{n=1}^{M \times S} |(E^s_{meas})_n|^2}}, \quad (14)$$

where $X = [a_0, a_1, ..., a_P, b_1, b_2, ..., b_P]$.

E^s_{meas} and E^s_z are $M \times S$ dimensional vectors containing the scattered electric field measured and computed at each iteration, respectively. M and S represent the total number of receivers and incident angles, respectively.

The cost functional J gives a measurement on how close the inverted results approach the true shape function. Thus, the inverse problem can be recast into an optimization problem by minimizing the relative error function with the coefficients of the trigonometric series being the parameters to be optimized. In this work, the problem is resolved by applying optimization approaches, where the standard searching scheme PSO and its hybrid models are employed to minimize the function J.

It is significant to note that these algorithms are optimization methods applicable to any problem which requires an optimization. Thus, if one is confronted with a more practical reconstruction case like the reconstructing of conducting underground objects or located inside dielectric objects, which will change is the theoretical formulation of the scattered field which differs from that considered in our case where the object to be reconstructed is placed in free space.

Consequently, the effectiveness of these methods depends on the complexity level of the forward problem considering that the resolution of the inverse problem is generally based on minimization of a least squares criterion.

Introduction to PSO, SA, and EO

The three methods PSO, SA, and EO are well known in the literature; I will state a brief introduction while indicating the corresponding references.

Basic PSO algorithm

PSO is a population based stochastic optimization technique developed by Kennedy and Eberhart in 1995 [14], inspired by social behavior patterns of organisms that live and interact within large groups.

The trial solutions x_p are iteratively updated by using the following two-step scheme [26]:

$$v_p^{(k+1)} = \omega^{(k)} v_p^{(k)} + c1 \cdot r1(p_p - x_p^{(k)}) + c2 \cdot r2(g - x_p^{(k)}), \quad (15)$$

$$x_p^{(k+1)} = x_p^{(k)} + v_p^{(k)}, \quad (16)$$

where $\omega(k)$ is the inertia parameter, $c1$ and $c2$ are acceleration coefficients, and $r1$ and $r2$ are two random numbers distributed uniformly in [0,1].

p_p and g are the best solution achieved by the pth particle and by the whole swarm so far, respectively.

Simulated annealing (SA)

SA was proposed by Kirkpatrick, Gelatt, and Vecchi in 1983 [27–29]. It was one of the first minimization stochastic methods applied to electromagnetic imaging.

In this paper, the initial temperature is determined by the following empirical formula:

$$T_0 = -\frac{J_{max} - J_{min}}{\ln(0.1)}, \quad (17)$$

where J_{max} and J_{min} are the maximum and minimum values of the function J in the initial swarm, respectively.

At the start of SA most worsening moves may be accepted, but at the end only improving ones are likely to be allowed. This can help the procedure jump out of a local minimum.

Extremal optimization (EO)

EO algorithm [30] is proposed by Boettcher and Percus for a minimization problem. Each decision variable in the current solution X is considered "species". In this study, we adopt the term "component" to represent "species". In this work, the Gaussian mutation is adopted witch it performs with the following representation:

$$x'_k = x_k + N_k(0, 1), \quad (18)$$

where x_k and x'_k denote the k-th decision variables before mutation and after mutation, respectively. $N_k(0, 1)$ denotes a Gaussian random number with mean zero and standard deviation one.

Hybrid algorithms, PSOSA, and PSOEO

In this section, we present the two algorithms which both combine the advantages of PSO (that has a strong global search ability) with SA and EO (that have a strong local-search ability).

PSOSA hybrid algorithm

This hybrid approach makes full use of the exploration ability of PSO and the exploitation ability of SA and offsets the weaknesses of each other. Consequently, through introducing SA to PSO, this algorithm is capable of escaping from a local optimum. However, if SA is introduced to PSO at each iteration, the computational cost will increase sharply and at the same time the fast convergence ability of PSO may be weakened. In order to perfectly integrate PSO with SA, SA is introduced to PSO every K_{max} iterations if no improvement of the global best solution does occur. Therefore, the hybrid PSOSA approach is able to keep fast convergence (most of the time) thanks to PSO. To prevent the premature convergence of PSO, SA is applied to the best solution in the swarm found so far, each K_{max} iterations that is predefined to 20 according to our experimentations. According to [22], the hybrid PSOSA algorithm works as illustrated in Fig. 2.

PSOEO hybrid algorithm

In this subsection, we present the second hybrid algorithm PSOEO as it is already detailed in [23]. This hybrid approach
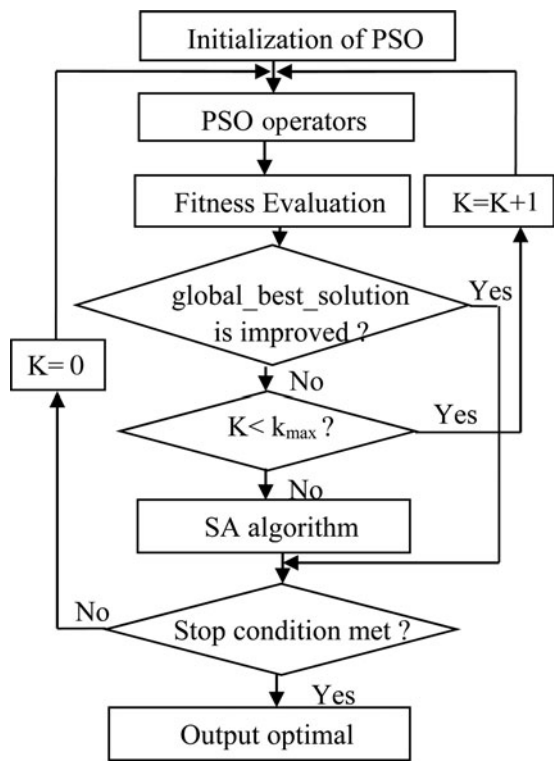
Fig. 2. PSOSA hybrid algorithm.

Fig. 3. Flowchart of the PSOEO algorithm, [23].

makes full use of the exploration ability of PSO and the exploitation ability of EO.

In order to perfectly integrate PSO with EO, EO is introduced to PSO every INV iterations. Therefore, the hybrid PSOEO approach is able to keep fast convergence in most of the time under the help of PSO. In our case, the value of INV is set to 10. According to [23], the hybrid PSOEO algorithm is illustrated in Fig. 3. It is important to note that, in order to find out the worst component (or so-called decision variable), each component of a solution should be assigned a fitness value in the EO procedure.

Numerical results

In this section, we discuss reconstruction results. We illustrate the performance of the hybrid algorithms and its sensitivity to random noise. The measurement is simulated by computation of the scattered field with preset electromagnetic parameters, making use the method of moments (MoM). The conducting object is illuminated by an incident TM wave at I illuminations equal to six positions $\varphi_i = (0, 30, 60, 90, 120, 150^{\circ})$, and the frequency is chosen to be 1 GHz.

For each illumination, the scattered electric field is collected at $M = 12$ points lying on a circle of radius $L = 2.5$ m and uniformly distributed around the investigation domain. The object which one will reconstruct its unknown shape is divided into 36 segments ($Q = 36$). The shape of the cylinder is expressed with Fourier coefficients ($P = 5$), the size of a particle is equal to $11 = 2P + 1$.

The initial values of the Fourier coefficients were chosen randomly (uniformly distributed in the range [−1, 1]). The initial values of the components of the particle velocities were also
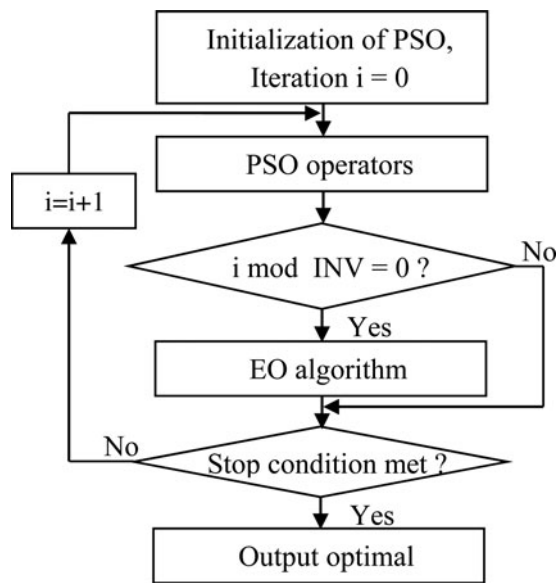
chosen randomly (uniformly distributed in the range [−0.2, 0.2]). The population size of the swarm N was selected equal to 60. The acceleration coefficients were selected constant ($c1 = c2 = 0.8$), whereas the inertia weight w decrease linearly starting from 1 to 0.5. For SA algorithm, the initial temperature T_0 is given by (17), annealing rate $\beta = 0.9$.

Four examples are investigated for the inverse scattering problem.

In the first example, a simple circular cylinder is examined, the shape function is chosen to be $\rho(\varphi) = (0.06)m$. The reconstructed shape function that corresponds to the best swarm particle is plotted in Fig. 4. The shape error is shown in Fig. 5. Here, the shape function discrepancy is defined as:

$$\text{SE} = \left\{ \frac{1}{Q} \sum_{q=1}^{Q} \left[\frac{\rho^{cal}(\varphi_q) - \rho(\varphi_q)}{\rho(\varphi_q)} \right]^2 \right\}^{\frac{1}{2}} \quad (19)$$

It is quite remarkable that the reconstructions are close to the exact shape of the object. However, it is clear that the best reconstructing is obtained by the hybrid algorithm PSOEO, indeed the shape error is of 10.3, 6.7, and 2.4% for PSO, PSOSA, and PSOEO, respectively. The convergence of the cost functional versus generations corresponding to the best particle in the swarm is shown in Fig. 6.

In the second example, we choose a shape function as $\rho(\varphi) = (0.05 + 0.02 \sin 4\varphi)m$. In order to investigate the sensitivity of these algorithms against random noise, a Gaussian white noise is added to the real and imaginary parts of the simulated scattered fields. The signal-to-noise ratio (SNR) of different levels is used in our simulations. Figures 7 and 8 present the reconstructed shape using the three algorithms and the shape error, respectively. Figure 9 shows the reconstructed results where the experimental scattered field is contaminated by noise. It could be observed that good reconstructions of the perfect conducting cylinder have been obtained when the SNR is above 15 dB.
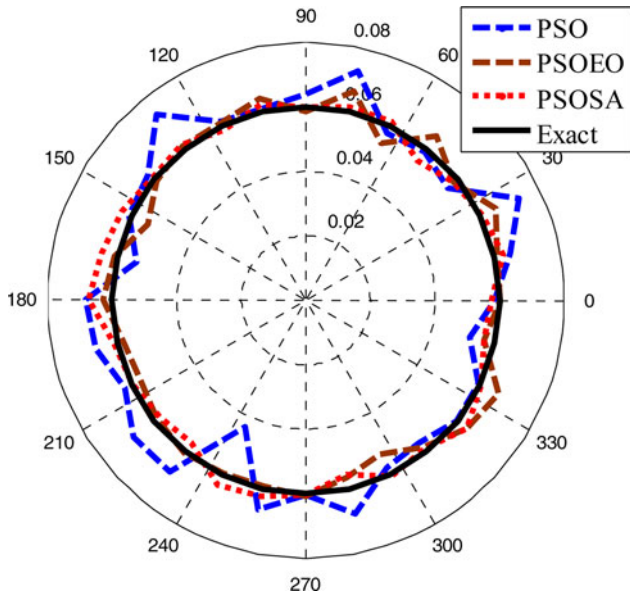
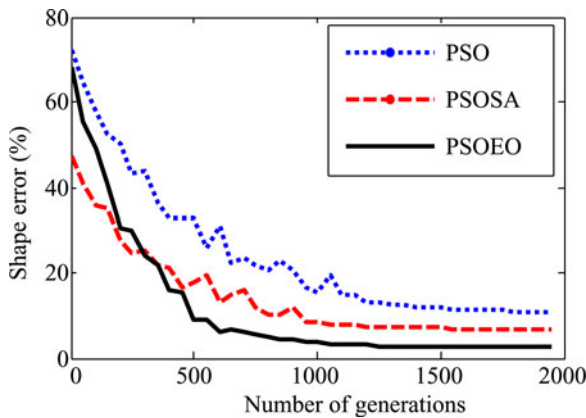**Fig. 4.** Reconstructed results for the first example.

Fig. 6. The cost functional versus generation.

Fig. 5. Shape function error in each generation.

Fig. 7. Reconstructed results for the second example.

Let us compare the three algorithms between them: it is clear that the two hybrid versions of PSO improved the reconstructing quality obtained by standard PSO. However, one observes that PSOEO is more effective than PSOSA algorithm especially against PSO, it presents less noise which is about 1.8% compared with 8.5 and 11.6% for PSOSA and PSO, respectively. Another advantage of PSOEO: it converges quickly, it put ~800 generations to reconstruct the object shape where more than 1200 iterations was necessary for the other algorithms.

Another test of the used methods seems very interesting when they will be executed several times on this same second configuration whose purpose is to observe the variation of SE. Figure 10 illustrates the performance SE according to the execution of the three techniques PSO, PSOSA, and PSOEO.

It is clear that the convergences lead practically to the same values of SE obtained previously which are 11.6, 8.5, and 1.8% for PSO, PSOSA, and PSOEO, respectively.

Finally, what we can conclude is that these methods efficiently explore the solution space and provide good coverage to the actual form of the original configuration.
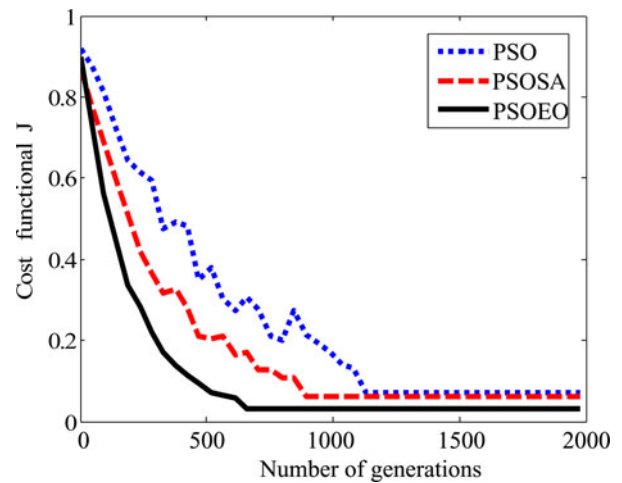
In [31], we developed a hybrid algorithm called mGA-CG combining a micro-GA and the method of the conjugate gradient. This technique allowed us to obtain good results for the reconstruction of the dielectric objects. It appears interesting to compare the performances of these different algorithms previously used with those of our own algorithm mGA-CG developed in [31]. To test the effectiveness of the algorithms as well as computing times, a third example is considered.

In the third example, the shape function is selected to be $\rho(\varphi) = (0.03 + 0.02 \sin \varphi + 0.01 \sin 3\varphi + 0.02 \cos \varphi)m$. Note that the shape function is not symmetrical about either x axis or y axis. For this example, the reconstruction results are given in Table 1.

This example has further verified the reliability and fast convergence of PSOEO compared with PSO and PSOSA. For PSOEO and mGA-CG algorithms, almost they led to the same results and there is not a great difference between them. From the three examples already considered, we can observe clearly that the PSOEO algorithm is more effective than PSO and PSOSA. Thus the following comparison will be carried out only between PSOEO and mGA-CG.
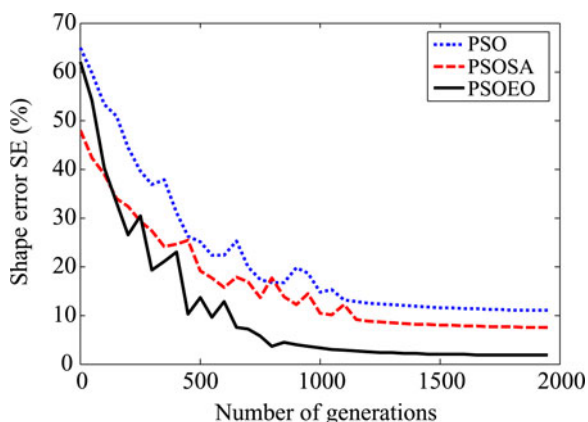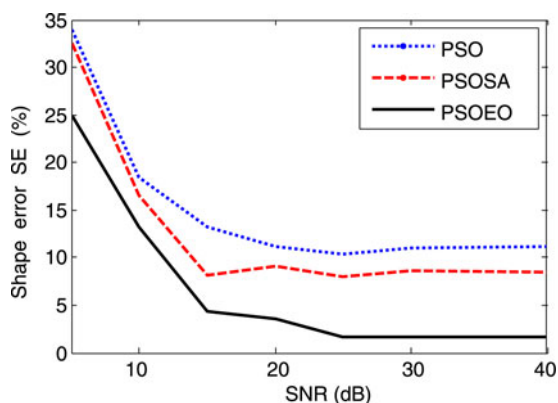
Fig. 8. Shape function error in each generation.

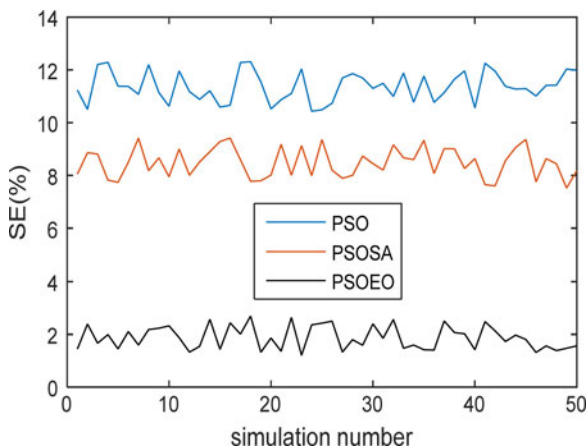**Fig. 9.** The shape error as a function of SNR (dB).

Fig. 10. The shape error for 50 simulations.

In the fourth example, the shape function is selected to be:

$$\rho(\varphi) = (0.05 + 0.02 \sin \varphi \cos^2 3\varphi)m.$$

The reconstructed shape function that corresponds to the best swarm particle found by the two algorithms is plotted in Fig. 11.

Table 1. Cost function, shape error, and computing time after convergence of algorithms for the third example

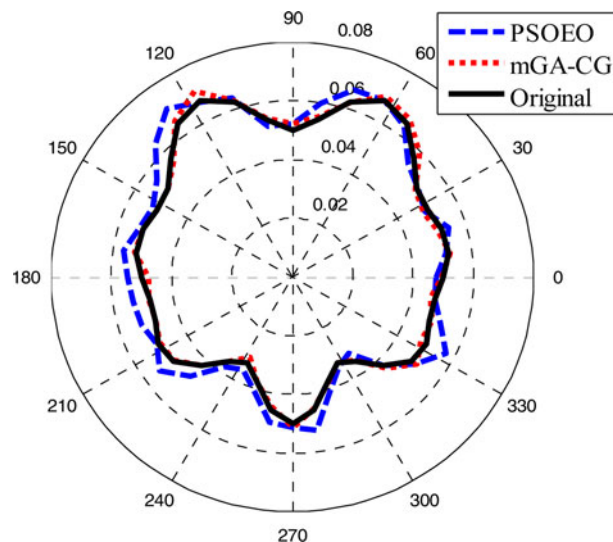|	PSO	PSOSA	PSOEO	mGA-CG [31]
J	0.12	0.092	0.047	0.042
SE (%)	7.42	3.26	0.84	0.78
Time (s)	1354	984	426	394

Fig. 11. Reconstructed results for the third example.

Table 2. Cost function, shape error, and computing time for the fourth example

	PSOEO	mGA-CG [31]
J	0.058	0.044
SE (%)	0.91	0.76
Time (s)	393	378

The fitness function, shape error, and computing time relative to each algorithm are given in Table 2.

From Fig. 11, we observe that the mGA-CG algorithm reconstructs the original contour of the object contrary to the PSOEO algorithm which converges to a contour presenting some deformations. Thus, we notice that the hybrid technique mGA-CG showed more effectiveness than PSOEO, but one can say that these two algorithms are comparable.

Let's analyze more the results found and especially the two presented techniques advantages. For all considered examples, the performances are very close. However, it does not preclude recalling that the mGA-CG method uses the gradient which is a local technique which cannot always guarantee the convergence of the latter toward the real solution. On the other hand, our two methods PSOSA and PSOEO combine global techniques only and thus a better chance to reach the desired solution. In order to complete the study of the two methods, it is very interesting to see the effect of certain parameters namely the measurement data size given by $m = M \times I$, the swarm size N, K_{max}, and
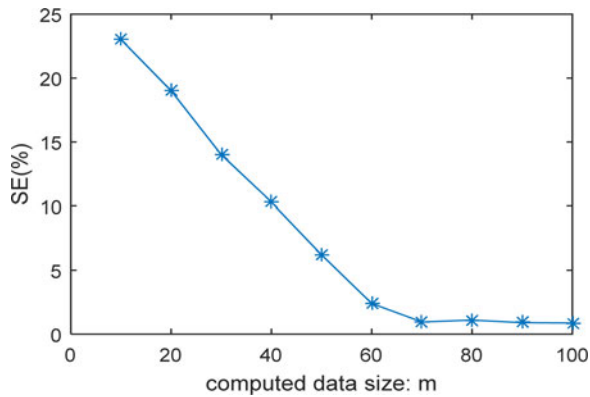
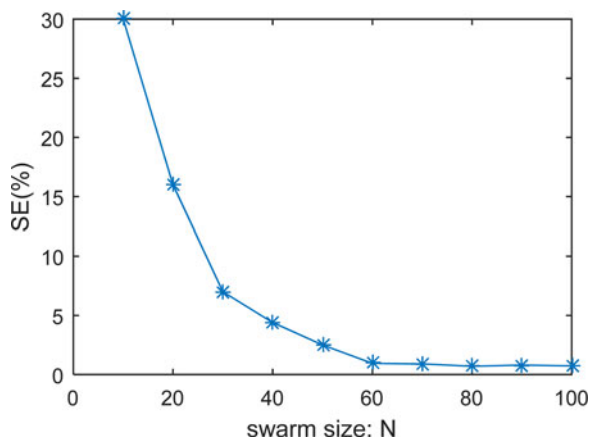**Fig. 12.** Shape error versus measurement size.

Fig. 13. Shape error versus swarm size.

INV. The impact of these parameters is carried out on the fourth example studied previously.

As an evaluation performance, we selected the shape error SE to detect the effect of these parameters. Figures 12 and 13 show the shape error evolution as a function of the number of measuring points m and the swarm size N, respectively. It is clear that more the m or N increase more a better reconstruction is obtained. We note also that from certain values of m and N, there will be no remarkable improvements.

In order to properly evaluate the robustness and the favor that these two hybrid algorithms can provide, a comparison with SA and EO is made. The two performances computational cost SE and the calculation time will be carried out during the reconstruction of the fourth case.

Table 3 shows the results of simulations obtained for the four algorithms, PSOSA, PSOEO, SA and EO. It is clear that PSOEO converges better compared with others and more robust than PSOEO for both performances. If we compare the hybrid methods with those with single agent (SA and EO), it is shown that SA and EO are faster while hybridization has improved the quality of reconstruction. So there is a tradeoff between computing time and computational cost.

Another simulation of K_{max} and INV effects is performed. Table 4 illustrates the simulation results for shape error by applying the two PSOSA and PSOEO techniques while varying K_{max} and INV respectively. From these results, we can notice that for

Table 3. Shape error and computing time after convergence of algorithms for the fourth example

	PSOSA	PSOEO	SA	EO
SE (%)	1.74	0.91	7.6	6.8
Time (s)	520	393	123	182

Table 4. Shape error for different values of K_{max} and INV for the fourth example

K_{max}	SE (%)	INV	SE (%)
10	3.5	10	2.9
20	2.5	20	2.3
30	1.2	30	1.6
40	0.8	40	1.4
50	1.0	50	0.9
60	1.2	60	1.1
70	1.3	70	1.4

low values of K_{max} and INV or from a certain threshold the SE becomes large. A better choice of K_{max} for PSOSA and INV for PSOEO should be around 40 and 50, respectively.

Conclusion

Two hybrid optimization methods called PSOSA and PSOEO for reconstructing the shape of perfectly conducting cylinders by TM waves have been employed. The forward problem is solved by using the MoM and the contour of the cylinder is approximated by Fourier series expansion. The computational results indicate that the algorithms appear to produce very good reconstructions of the object shape from the scattered fields even in the presence of the measurement noises. Compared with standard PSO and PSOSA, it has been shown that the PSOEO approach has better performances in terms of accuracy, convergence rate, stability, and robustness. The PSOEO algorithm is also compared with our own technique named mGA-CG and a superiority of this last method concerning the precision and the convergence speed is recorded. However, these illustrated algorithms are random and to support one compared with another requires a sufficient number of tests and evaluations. Finally, these two techniques can be regarded as a powerful optimization tool for the electromagnetic problems especially in microwave imaging.

References

1. **HoLmann B and Scherzer O** (1994) Factors influencing the illposedness of nonlinear problems. *Inverse Problems* **10**, 1277–1297.
2. **Qing A and Jen L** (1997) A novel method for microwave imaging of dielectric cylinder in layered media. *Journal of Electromagnetic Waves and Applications* **11**, 1337–1348.
3. **Van den berg PM and Van der Horst M** (1995) Nonlinear inversion in induction logging using the modified gradient method. *Radio Science* **30**, 1355–1369.

4. **Garnero L, Franchois A, Hugonin JP, Pichot C and Joachimowicz N** (1991) Microwave imaging-complex permittivity reconstruction-by simulated annealing. IEEE Trans. *Microwave Theory and Techniques* **39**, 1801–1807.

5. **Brovko Alexander V, Murphy Ethan K and Yakovlev Vadim V** (2009) Waveguide microwave imaging: neural network reconstruction of functional 2-D permittivity profiles. *IEEE Transactions on Microwave Theory and Techniques* **57**, 406–414.

6. **Chien W** (2008) Inverse scattering of an un-uniform conductivity scatterer buried in a three-layer structure. *Progress in Electromagnetics Research, PIER* **82**, 1–18.

7. **Krraoui H, Mejri T and Aguili T** (2016) Dielectric constant measurement of materials by a microwave technique: application to the characterization of vegetation leaves. *Journal of Electromagnetic Waves and Applications* **30**, 1643–1660.

8. **Chiu C-C and Liu P** (1996) Image reconstruction of a perfectly conducting cylinder by the genetic algorithm. *IET Microwaves, Antennas & Propagation*, **143**, 249–253.

9. **Qing A** (2006) Dynamic differential evolution strategy and applications in electromagnetic inverse scattering problems. *IEEE Transactions on Geoscience and Remote Sensing* **44**, 116–125.

10. **Rekanos I** (2008) Shape reconstruction of a perfectly conducting scatterer using differential evolution and particle swarm optimization. *IEEE Transactions on Geoscience and Remote Sensing* **46**, 1967–1974.

11. **Semnani A, Rekanos IT, Kamyab M and Papadopoulos TG** (2010) Two-dimensional microwave imaging based on hybrid scatterer representation and differential evolution. *IEEE Transactions on Antennas and Propagation* **58**, 3289–3298.

12. **Rocca P, Benedetti M, Donelli M, Franceschini D and Massa A** (2009) Evolutionary optimization as applied to inverse scattering problems. *Inverse Problems in Science and Engineering* **25**, 123003–1–123003–44.

13. **Rocca P, Oliveri G and Massa A** (2011) Differential evolution as applied to electromagnetics. *IEEE Transactions on Antennas and Propagation* **53**, 38–49.

14. **Kennedy J and Eberhart RC** (1995) Particle swarm optimization. *Proceedings of IEEE International Conference on Neural Networks* **4**, 1942–1948.

15. **Huang C-H, Chiu C-C, Li C-L and Chen K-C** (2008) Time domain inverse scattering of a two-dimensional homogenous dielectric object with arbitrary shape by particle swarm optimization. *Progress in Electromagnetics Research, PIER* **82**, 381–400.

16. **Donelli M and Massa A** (2005) Computational approach based on a particle swarm optimizer for microwave imaging of two-dimensional dielectric scatterers. *IEEE Transactions on Microwave Theory and Techniques* **53**, 1761–1776.

17. **Semnani A and Kamyab M** (2008) Truncated cosine Fourier series expansion method for solving 2-D inverse scattering problems. *Progress in Electromagnetics Research, PIER* **81**, 73–97.

18. **Randazzo A** (2012) Swarm optimization methods in microwave imaging. *International Journal of Microwave Science and Technology* **2012**, Article ID 491713, 12.

19. **Kumar A, Bhattacharya A and Singh DK** (2013) Microwave image reconstruction of two dimension dielectric scatterers using swarm particle optimization. *IJECET* **4**, 57–61.

20. **Chiang J-S, Gu W-S, Chiu C-C and Sun C-H** (2015) Estimation of the two-dimensional homogenous dielectric scatterer in a slab medium using particle swarm optimization and asynchronous particle swarm optimization. *Research in Nondestructive Evaluation* **26**, 208–224.

21. **Bindu G and Mathew KT** (2004) Characterization of behind and malignant breast tissues using 2-D microwave tomographic imaging. *Microwave and Optical Technology Letters* **49**, 2341–2345.

22. **Suganthan PN, Hansen N, Liang JJ, Deb K, Chen Y-P, Auger A and Tiwari S** (2005) Problem Definitions and Evaluation Criteria for the CEC 2005 Special Session on Real-Parameter Optimization, Technical Report, Nanyang Technological University, Singapore and IIT Kanpur, India.

23. **Chen M-R, Li X, Zhang X and Lu Y-Z** (2010) A novel particle swarm optimizer hybridized with extremal optimization. *Applied Soft Computing* **10**, 367–373.

24. **Harrington RF** (1993) *Field Computation by Moment Method*. New York, USA: Wiley IEEE Press.

25. **Tezel NS and Şimşek S** (2007) Neural network approach to shape reconstruction of a conducting cylinder. *Journal of Electrical & Electronics Engineering* **7**, 299–304.

26. **Ülker ED and Ülker S** (2014) Application of particle swarm optimization to microwave tapered microstrip lines. *CSEIJ* **4**, 59–64.

27. **Kirkpatrick S, Gelatt Jr CD and Vecchi MP** (1983) Optimization by simulated annealing. *Journal of Science* **220**, 671–680.

28. **Taheri J and Zomaya AY** (2005) A simulated annealing approach for mobile location management. *Proceedings of the 19th IEEE International Parellel and Distributed Processing Symposium (IPDPS)*.

29. **Suman B and Kumar P** (2006) A survey of simulated annealing as a tool for single and multi-objective optimization. *Journal of the Operational Research Society* **57**, 1143–1160.

30. **Boettcher S and Percus AG** (2000) Nature's way of optimizing. *Artificial Intelligence* **119**, 275–286.

31. **Mhamdi B, Grayaa K and Aguili T** (2011) Microwave imaging of dielectric cylinders from experimental scattering data based on the genetic algorithms, neural networks and a hybrid micro genetic algorithm with conjugate gradient. *International Journal of Electronics and Communications* **65**, 140–147.

Bouzid Mhamdi was born in Kasserine, Tunisia, on June 7, 1977. He received his electrical engineering degree (2002) and M.Sc. (2004), and Ph.D. (2011) in telecommunication from the National Engineers School of Tunis, Tunisia. At present, he works at the University of Kairouan, ISSAT Kasserine as an Associate Professor in Communications Engineering Department. His current research interests include forward and inverse electromagnetic problems for microwave imaging and MIMO systems.